

AUG 8 1979

NAS 1.60:1492

COMPLETED

NASA Technical Paper 1492

ORIGINAL

Contoured Tank Outlets for Draining of Cylindrical Tanks in Low-Gravity Environment

Eugene P. Symons

JULY 1979

NASA

46

NASA Technical Paper 1492

Contoured Tank Outlets for Draining of Cylindrical Tanks in Low-Gravity Environment

Eugene P. Symons
*Lewis Research Center
Cleveland, Ohio*



National Aeronautics
and Space Administration

**Scientific and Technical
Information Branch**

SUMMARY

This report presents the results of an investigation that included the analysis, fabrication, and subsequent testing of two small-scale hemispherical-bottomed cylindrical tanks in which the outlets were contoured to prevent vapor ingestion when the tanks are drained in a low-gravity environment. Liquid residuals in the contoured tanks at vapor ingestion were compared with those in a tank with a conventional outlet having a constant circular cross-sectional area. The contoured-outlet tank drained nearly completely before vapor ingestion when it was drained at design conditions. Even when drained at off-design conditions (i.e., different outflow rates, fluids, gravitational environments, etc.), the contoured-outlet tank had lower residuals than a hemispherical-bottomed tank with a conventional outlet. Additionally, the effects of viscosity, outflow rate, and gravitational environment were considered. The analysis was also applied to tanks that might be used for in-orbit supply of a cryogenic tug.

INTRODUCTION

The Lewis Research Center has conducted studies of various phenomena occurring when containers are drained in a low-gravity environment. These studies have examined liquid-vapor interface distortion, vapor ingestion, liquid residuals, and several methods that might be used to reduce liquid residuals at vapor ingestion. References 1 and 2 examined the distortion of the liquid-vapor interface during the draining process in weightlessness and found that the magnitude of the distortion was dependent on the outflow Weber number and the initial filling level and independent of the tank bottom shape for the cylindrical tanks tested. Reference 3 determined the critical and vapor ingestion heights (as well as the corresponding liquid residuals) in both normal gravity and weightlessness for a flat-bottomed cylindrical tank. Reference 4 performed a similar study for hemispherical-bottomed tanks. In these studies, the vapor ingestion height correlated with the Froude number in normal gravity, and the critical height correlated with the Weber number in weightlessness.

The severe distortion of the liquid-vapor interface during draining in a low-gravity environment results in large liquid residuals. Thus, more recent studies have examined various methods that might be used to reduce liquid residuals. References 5 and 6 considered the use of simple baffles placed over the outlet line in cylindrical tanks with

flat and hemispherical bottoms, respectively. Reference 7 examined the use of outflow-rate throttling during draining.

This study examines another technique, that of contouring or shaping the outlet region in such a fashion that vapor ingestion into the outlet does not occur. This concept is not a recent development and has been demonstrated in normal gravity. Some earlier analytical and experimental work is reported in references 8 and 9, in which the governing equations were developed and some tests performed in normal gravity. The present report presents the analysis and applies that analysis to the design and fabrication of two small-scale cylindrical tanks. These tanks were then tested in the Lewis Research Center's Zero Gravity Facility in a low-gravity environment in order to evaluate the analytical model in terms of the predicted draining performance. Once the liquid, outflow rate, and gravitational environment were specified, the outlet contour could be uniquely determined. Draining tests were first performed with the same liquid, outflow rate, and gravitational environment as used for the tank design. Additional tests were then made with other liquids, gravitational environments, and outflow rates in order to determine empirically how these variables would affect the overall draining performance. Liquid residuals were determined for each test and compared with those to be expected if the tank outlet was not contoured (i. e., when it had an outlet line of constant circular cross-sectional area located along the tank axis). Effects of fluid properties, gravitational environment, and outflow rate on the predicted outlet contour are discussed. Two potential applications of contouring are presented.

SYMBOLS

A_1	parameter, $2Q^2/\pi^2$, cm^6/sec^2
a	inertial acceleration, cm/sec^2
B_1	parameter, $4\mu\pi/\rho Q$, $1/\text{cm}$
Bo	Bond number, aR_T^2/β
C	constant
D	diameter, cm
F	viscous loss at wall, cm^2/sec^2
Fr	Froude number, $Q^2/\pi^2 a R_T^5$
f	friction factor
G	total acceleration, cm/sec^2
g	gravitational acceleration, cm/sec^2

h	axial distance from reference point, cm
P	pressure, $\text{g}/\text{cm} \cdot \text{sec}^2$
P_0	reference pressure, $\text{g}/\text{cm} \cdot \text{sec}^2$
Q	volumetric outflow rate, cm^3/sec
R_T	tank radius, cm
Re	Reynolds number, $\rho V D / \mu$
r	outlet-contour radius, cm
S	slope
T	slope of conical segment, $dh/-dr$
t	time, sec
V	dimensionless volume of liquid residual
v	velocity, cm/sec
v_h	axial component of velocity, cm/sec
v_r	radial component of velocity, cm/sec
v_s	velocity along streamline, cm/sec
We	Weber number, $Q^2/\pi^2 \beta R_T^3$
z	axial distance from hemispherical origin, cm
α	angle, deg
β	specific surface tension, cm^3/sec^2
θ	angle, deg
μ	viscosity, $\text{g}/\text{cm} \cdot \text{sec}$
ρ	density, g/cm^3
σ	surface tension, dynes/cm

CONTOURED-OUTLET ANALYSIS

Vapor ingestion caused by suction dip into the outlet line during outflow from a tank will not occur if the draining liquid remains in its equilibrium configuration (as determined by the Bond number, the tank shape, and the contact angle) as it passes into and through the outlet line. In general, this objective could be achieved if the axial component of the velocity had no radial dependence at any fixed axial position in the tank or in

the outlet. To achieve this objective, we seek an appropriate contour or shaping of the tank outlet region. A general outlet configuration (including a portion of the tank) is shown in figure 1, along with the pertinent variables. The approach used herein is similar to that used in reference 9, except for the approach used in treating the static-pressure drop in the outlet. Both analyses thus neglect the effect of surface tension.

By assuming that the liquid to be drained is incompressible and that only conservative body forces act on the liquid, we write the Bernoulli equation with friction between a point on the liquid-vapor interface and a point in the tank outlet region adjacent to the tank wall. Then, by differentiating that equation (assuming the flow is uniform at each axial location and using the Darcy-Weisbach equation for pipe flow), we arrive at an equation for the tank outlet contour for the case in which the static pressure remains constant as the flow passes into and through the outlet line. The equation is

$$\frac{dT}{dr} + \frac{2T}{r} (1 + T^2) \left[1 + \frac{f}{8} (1 + T^2)^{1/2} \right] - T^4 \left(\frac{G\pi^2 r^4}{Q^2} \right) = 0 \quad (1)$$

By assuming that the outlet consists of a large number of frustums of cones (fig. 2), this equation can further be reduced to

$$r^5 = \frac{A_1}{T^3 G} (1 + T^2) \left(1 + B_1 r \sqrt{1 + T^2} \right) \quad (2)$$

For the case in which a static-pressure drop equal to the hydrostatic head is permitted as the flow passes into and through the outlet line, these equations become

$$\frac{dT}{dr} + \frac{2T}{r} (1 + T^2) \left[1 + \frac{f}{8} (1 + T^2)^{1/2} \right] - \frac{\pi^2 r^4 T^3}{Q^2} \left(GT + \frac{1}{\rho} \frac{dP}{dr} \right) = 0 \quad (3)$$

and

$$r^5 = \frac{A_1}{2GT^3} (1 + T^2) \left(1 + B_1 r \sqrt{1 + T^2} \right)$$

Details of the analysis and the method of solving these equations are presented in appendix A.

NUMERICAL RESULTS

A computer program based on an iteration technique was written to solve the equations developed in appendix A and presented in the previous section. This program was then used to investigate the effects of the pertinent variables on the tank outlet contour.

The solutions to the equations presented yielded the outlet-contour radius r as a function of the axial position h from some reference point $h = 0$ at which r was taken to be equal to the tank radius. The contours plotted in figures 3 to 5 show r as a function of the axial position z measured from the origin of the original hemispherical tank bottom O' . The contours as plotted were determined by alining the axis of the original tank with the axis of the predicted outlet contour and graphically positioning the contour so it was nearly tangent to the hemispherical bottom of the original tank. Thus, $z = h + C$, where C is the axial position of the initial $h = 0$ point (fig. 1).

Since it was anticipated that this study would eventually culminate in an experimental program, the effect of varying the kinematic viscosity ratio μ/ρ was evaluated numerically from the properties of the test liquids used in previous experimental draining studies. By selecting, as the two test liquids, ethanol and a mixture of 60 percent ethanol and 40 percent glycerol by volume, it was possible to obtain a 10:1 variation in kinematic viscosity. The numerical predictions of the outlet contour for a 2-centimeter-radius tank with a constant outflow rate of 20 cubic centimeters per second and a constant gravitational environment of 0.015 g are presented in figure 3 for a tank in which the static pressure is constant as flow passes through the outlet line. Similar results were obtained for a 3-centimeter-radius tank with a constant outflow rate of 30 cubic centimeters per second and a constant gravitational environment of 0.015 g. As shown in figure 3, the 10:1 variation in kinematic viscosity had only a small effect on the outlet configuration for the flow rate shown, resulting in a maximum increase in radius of approximately 5.5 percent. Furthermore, the numerical data of reference 8 also show that viscosity had relatively little effect on the outlet design.

The effect of varying the gravitational environment for constant fluid properties (ethanol) and constant outflow rate ($20 \text{ cm}^3/\text{sec}$) is shown in figure 4 for a 2-centimeter-radius tank. A 62.5:1 variation in gravity level significantly changed the required contour, resulting in a maximum increase in radius of 110 percent at the flow rate shown. Furthermore, as the gravity level decreased toward zero g, the outlet radius approached the tank radius. Thus contouring would be impractical for draining in weightlessness.

The effect of a 4:1 variation in outflow rate is shown in figure 5 for fixed liquid properties (ethanol), tank size (2 cm radius), and gravitational environment (0.015 g). Again, this variation significantly changed the predicted contour, resulting in a maximum increase in radius of approximately 64 percent.

It can be concluded from figures 3 to 5 that, in planning an experimental program, the test liquid can be chosen without regard to kinematic viscosity but both the gravitational environment and the outflow rate, which significantly affect the outlet contour, must be carefully selected to provide an outlet with a reasonable shape. (A reasonably shaped outlet is arbitrarily defined as an outlet whose final radius is less than 1/5 the tank diameter at a distance of 1 tank diameter from the origin of the original hemispherical bottom.)

APPARATUS

The Lewis Research Center's Zero Gravity Facility was used to obtain the experiment data for this investigation. The facility, the experiment vehicle, and the test procedure are described in detail in appendix B.

Experiment Tanks

The experiment tanks used in this study are shown in figure 6. The tanks were cylindrical in cross section, machined from cast acrylic plastic, and polished for optical clarity. Two tanks were designed: one with an inside radius of 2 centimeters and the other, 3 centimeters. The outlet contour was determined from the numerical solution of the equations presented in the section CONTOURED-OUTLET ANALYSIS for the case where no static-pressure drop is permitted in the outlet. It was assumed that ethanol was the test liquid, that the gravitational environment was 0.015 g (maximum obtainable in the facility), and that the outflow rates were 20 cubic centimeters per second for the 2-centimeter-radius tank and 30 cubic centimeters per second for the 3-centimeter-radius tank (the minimums obtainable due to time constraints in the facility). The top and bottom of each tank were plates machined from stainless steel and equipped with O-rings to provide a positive seal. Each tank had a cylindrical pressurant-gas inlet and a liquid-outlet line, both of which were located along the tank axis. At the pressurant-gas inlet, each tank was fitted with an air-deflector baffle having a diameter equal to the tank radius. This baffle was positioned 1/2 tank radius from the top of the tank and prevented direct impingement of the pressurant gas onto the liquid-vapor interface during draining.

Test Liquids

The liquids used in this investigation and their pertinent physical properties are presented in table I. To improve the photographic quality of the data films, a small

quantity of dye was added to each liquid. The dye had no measurable effect on the fluid properties. The liquids were chosen to provide a range of about 35:1 in kinematic viscosity ratio μ/ρ ; their properties correspond to those of liquids that had been used in other draining studies.

EXPERIMENT RESULTS AND DISCUSSION

Interface Motion During Draining

When a tank enters a low-gravity environment from a normal-gravity environment, the liquid-vapor interface undergoes a transition in which it moves from a nearly flat configuration in normal gravity (high Bond number) to a highly curved configuration in low gravity (low Bond number). Typically, the interface oscillates about its final equilibrium configuration for a period of time that depends on tank size, specific surface tension, and viscosity. Since the time to reach final equilibrium exceeds the time available in drop towers, even for the relatively small tanks used in this study, outflow was begun when the center of the liquid-vapor interface reached the lowest point during its first oscillation. The liquid-vapor-interface centerline velocity at this time was zero. Although this time has been empirically correlated for weightlessness ($t = 0.146 (\rho/\sigma)^{1/2} D^{3/2}$, ref. 10), to the author's knowledge this information does not exist for low-gravity environments. Therefore, a series of preliminary tests were performed to determine this time for the tanks and liquids used in this study at the design gravity level of 0.015 g. The results of those tests are summarized in table II.

In previous draining studies (refs. 1 to 7), the outflow rates were sufficient for the inertia forces to dominate the interface motion, and the liquid-vapor interface proceeded to move smoothly after outflow was begun. In this study, to achieve an acceptable outlet contour (arbitrarily chosen as a final outlet-contour radius of less than 1/5 the tank diameter), we had to design the tanks to drain at lower outflow rates than had been the case in previous drop-tower tests. This resulted in correspondingly low outflow Weber numbers (the ratio of the relative importance of inertia to capillary forces). Hence, the interface motion was not dominated by inertia. Thus, even after outflow was begun, when the interface had reached the lowest point in its first pass through equilibrium, the interface oscillations continued throughout the draining process. These oscillations apparently had little effect on the results. This contention was supported by the low liquid residuals and by the lack of a measurable change in the magnitude of the liquid residuals in several tests where the outflow was begun at various times both before and after the liquid-vapor interface had reached the lowest point in its first pass through equilibrium. However, for consistency and easy comparison with previous studies, all the data pre-

sented herein were obtained by beginning draining when the liquid-vapor interface had reached the lowest point in its first pass through equilibrium.

Determination of Liquid Residuals

In this report, liquid residuals are defined as the quantity of liquid remaining in the tank when the liquid-vapor interface passes the plate located at the bottom of the tank outlet. Residuals were then determined by subtracting the calculated drained liquid volume from the initial liquid volume.

To simplify testing procedures, initial liquid volumes were determined by sealing the tank outlet (at the plate) and measuring the volume of liquid added to the tank with a graduated cylinder. As each measured volume was added to the tank, the corresponding height from the plate was read from a scale mounted parallel to the longitudinal tank axis and adjacent to the tank. In this fashion, initial volume as a function of liquid height was determined for each tank.

The total volume of liquid drained was calculated by taking the product of the draining time and the steady-state outflow rate. The outflow rate was determined from a normal-gravity calibration test in which interface displacement was measured as a function of time. The low-gravity outflow rate was assumed to equal the normal-gravity outflow rate, an assumption that had been verified in weightlessness (ref. 2). This equality of outflow rates was primarily due to the negligible change in liquid heads in relation to the supply tank pressure. Additionally, a drag-body flowmeter was used to check the magnitude of the outflow rate. In those tests in which the Reynolds numbers were high enough to provide accurate data from the flowmeter (excluding all runs with the high-viscosity liquid), the data taken from the plot of normal-gravity interface displacement with time agreed quite well with data taken from the flowmeter (generally within ± 5 percent).

These methods of calculating liquid residuals necessarily involved some uncertainty. For example, since the initial heights could only be accurately determined just before a test to within ± 0.1 centimeter, the initial liquid volumes could conceivably have been in error by as much as ± 2.82 cubic centimeters in the larger tank and ± 1.26 cubic centimeters in the smaller tank. Furthermore, since draining was begun by operating an electrically driven solenoid valve, some transient was involved during which the outflow rate increased from zero to its final steady-state value. Thus, some uncertainty was inherent in the manner in which the volumes of liquid drained were determined. During this initial transient phase (nominally about 30 msec), the outflow rate was assumed to vary linearly with time from zero to its steady-state value. It was anticipated that such an approximation would result in a negligible error. Additionally, the time at which the solenoid valve was opened was preset by adjusting time delay relays on board the pack-

age. This time was determined during a test by reading the digital clock when a light wired in series with the solenoid valve and located in the camera's field of view was activated. This time could also be obtained from the flowmeter output. In general, the times agreed almost exactly, and this source of error was not considered.

In conclusion, the methods used to calculate liquid residuals permitted an uncertainty of ± 2.8 cubic centimeters in the larger tank and ± 1.26 cubic centimeters in the smaller tank. For easier comparison with previous draining studies (refs. 4 and 11), this uncertainty can be expressed in nondimensional form in terms of the volume \bar{V} that is contained in a hemisphere with the tank radius. Thus $\bar{V} = (\text{Liquid residual})/(\text{Volume of hemisphere})$, and the maximum uncertainty in calculating \bar{V} is ± 0.050 in the larger tank and ± 0.075 in the smaller tank. The experiment data are summarized in table III, where the calculated residuals are expressed in nondimensional form. Additionally, the final column in the table presents an estimate of the nondimensional liquid residual from the draining of a noncontoured, hemispherical-bottomed tank with a circular cross-sectional outlet under identical conditions. The values shown were obtained from references 4 and 11 for zero- and low-gravity conditions, respectively.

Draining at Design Conditions

As previously discussed, the outlet contours for the tanks used in these experiments were designed from the numerical solution of the equations presented in the section CONTOURED-OUTLET ANALYSIS. Ethanol was the test liquid. The outflow rates were 20 cubic centimeters per second for the 2-centimeter-radius tank and 30 cubic centimeters per second for the 3-centimeter-radius tank. The gravitational environment was fixed at 0.015 g. And the static pressure in the outlet was constant. Therefore, if the developed equations were correct and if the tests were performed at the design conditions (i.e., ethanol at 0.015 g and the appropriate outflow rate), all the liquid should have drained from the tanks before vapor was ingested.

After both the larger tank and the smaller tank had been drained at the design conditions, it first appeared that all the liquid had drained out. However, close examination of the data films showed a small liquid layer adjacent to the tank walls at vapor ingestion. The existence of this layer could be verified at the conclusion of the test, when the experiment package was decelerated. The behavior of the liquid-vapor interface during draining at the design conditions is shown in figure 7 for both tanks.

Examining the calculated values of nondimensional residuals \bar{V}_r at the design conditions in table III shows that, in both the larger and smaller tanks, the residuals were less than would be predicted to occur at the same conditions without outlet contouring. However, in neither case was the residual in the contoured-outlet tank calculated to be zero, although its absolute value was quite small (i.e., 6.22 cm^3 in the larger tank and

5.03 cm³ in the smaller tank.) This result was not wholly unexpected since the no-slip condition at the tank wall gives rise to the formation of a thin boundary layer. Nor is it surprising that such a small volume would be difficult to detect since, if it were contained in a thin wall layer uniformly distributed along the tank wall, it would be less than 0.1 centimeter thick. Furthermore, this layer would probably remain very thin as tank size is increased, resulting in a smaller residual volume for larger tanks.

Effect of Viscosity on Liquid Residuals

From the computer solutions of the equations, it was anticipated that the outlet contour would not be significantly altered if a more viscous liquid were used. Hence, residuals from all the liquids used in this study, regardless of viscosity, should be comparable if the outflow rate and gravitational environment were held constant. To verify this contention, several draining tests were made with both trichlorotrifluoroethane and a mixture of 60 percent ethanol and 40 percent glycerol. These liquids had a ratio in kinematic viscosity of 35:1. The behavior of the liquid-vapor interface during draining is shown in figure 8 for the very viscous ethanol-glycerol mixture. The greater viscosity did not result in any noticeable increase in liquid residuals over those for the same tank with ethanol (fig. 7(b)). However, increasing the viscosity did appear to increase the quantity of calculated residuals (table III). Again this is probably due to the thicker boundary layer that would occur with the more viscous fluid.

Effect of Gravitational Environment on Liquid Residuals

From the computer results, it was expected that any change in gravitational environment would necessitate that the outlet contour be significantly altered to permit complete draining. Additionally, it was anticipated from the equations that for draining in zero gravity, the outlet size would have to approach the tank size. This would imply that contouring the tank outlet to achieve complete draining in zero gravity is not practical.

To assess the performance of the contoured-outlet tank under such conditions, each tank was tested with ethanol at the design outflow rate (nominally 20 cm³/sec in the smaller tank and 30 cm³/sec in the larger tank) in weightlessness. Again, the photographic data indicated that the residuals were greater in weightlessness than in the design gravitational environment of 0.015 g. This indication was confirmed by the calculated residuals shown in table III. The residuals calculated for the contoured-outlet tank in weightlessness (Bond number of 0) were still lower than those that were predicted to occur in weightlessness for a conventional-outlet tank.

An additional test was conducted with ethanol at a nominal outflow rate of 30 cubic centimeters per second in the larger tank at a gravity level of 0.007 g. The calculated residual for this case (table III) was slightly greater than that which occurred at the design gravity level of 0.015 g but still considerably less than would be expected if the tank outlet had not been contoured.

A typical test result in weightlessness is shown photographically in figure 9. Compare the liquid residuals for this test with those shown in figure 7(b), in which the conditions were identical except for the gravitational environment.

Effect of Outflow Rate on Liquid Residuals

The numerical results show that the outflow rate should have a significant effect on the outlet contour; thus, it was assumed that draining at outflow rates in excess of design would result in some sizeable increase in liquid residuals. To verify this assumption, outflow rates approximately 8.4 times the design value of 30 cubic centimeters per second were run in the 3-centimeter-radius tank, and outflow rates approximately 5.2 times the design value of 20 cubic centimeters per second were run in the 2-centimeter-radius tank, each at the design gravitational environment of 0.015 g. The results are shown photographically in figure 10. Again, compare the liquid residuals from this test with those shown in figure 7(a), in which the conditions were the same except for the outflow rate. These observed results were confirmed by the calculated liquid residuals shown in table III. As the outflow rate (i.e., Weber number) was increased at a constant Bond number, the corresponding calculated liquid residuals also increased. Also, even at an outflow rate in excess of design, the calculated liquid residuals were consistently lower than would have been predicted for the same conditions if the tank had not been contoured.

POTENTIAL CONTOUR APPLICATIONS

As part of a recent study (ref. 12), several in-orbit fluid transfer systems most likely to benefit by efficient and predictable in-orbit fluid supply were conceptually defined. In that study, the supply modules were assumed to be payloads of the space shuttle, and the space tug was taken to be representative of a high-energy upper stage requiring large quantities of cryogenic fluids. Two of the four systems defined used linear acceleration provided by small thrusters or by drag and involved resupply of a cryogenic tug. It is these systems that lend themselves to outlet contouring as a means of reducing propellant residuals.

The first system consists of a tug in-orbit supply with the tug and the supply module separated from the shuttle. The operating characteristics of the system are presented in detail in reference 12, and the discussion herein is restricted to describing the tank outlet region if outlet contouring were used instead of the outlet baffles described in reference 12. In defining the tank outlet region, the tank diameters, the acceleration environment of 10^{-4} g's (obtained by using a thruster), and the transfer time of 2.5 hours were retained as were the approximate overall tank length and volume. Using these parameters in the equations presented in the section CONTOURED-OUTLET ANALYSIS resulted in the tank contouring described in figure 11 both for constant static pressure in the outlet line and for a static-pressure drop (as per appendix A). Both the liquid-oxygen and the liquid-hydrogen tanks were approximately 10.7 meters (421 in.) long with respective inside diameters of 1.52 and 2.64 meters (59.8 and 103.9 in.). The outlet region of the liquid-oxygen tank was terminated approximately 2 meters (78.7 in.) from the origin of the original hemispherical tank bottom. At this location the outlet diameter was 0.228 meter (8.98 in.) for constant static pressure in the outlet and 0.191 meter (7.52 in.) for a static-pressure drop (see equations in appendix A). The outlet region of the liquid-hydrogen tank was terminated approximately 2.9 meters (114 in.) from the origin of the original hemispherical tank bottom. At this location the outlet diameter was 0.369 meter (14.53 in.) for constant static pressure and 0.309 meter (12.17 in.) for a static-pressure drop.

The second system considered in reference 12 made use of the drag forces acting on the shuttle orbiter in a 296-kilometer (160-n mi) orbit to orient the liquid oxygen and hydrogen at the tank outlets. (Again for system operating details, see ref. 12). As in the separated system, the tank diameters were retained, as were the approximate overall tank lengths and volumes. In defining the outlet contour, an acceleration environment of 10^{-6} g and transfer times of 10, 20, and 30 hours were considered. (In ref. 12, a transfer time of 20 hr was chosen.) The resulting outlet configurations are shown in figure 11. In the 10-hour transfer mode, the outlet diameters were too large to be practical (i.e., 0.354 m at approximately 2.0 m from the origin of the hemispherical bottom in the liquid-oxygen tank and 0.572 m at approximately 2.8 m from the origin of the hemispherical bottom in the liquid-hydrogen tank). However, if some static-pressure drop was permitted (again as in appendix A), the outlet diameters at the same locations were reduced to 0.296 meter in the liquid-oxygen tank and 0.481 meter in the liquid-hydrogen tank.

In all cases, the 20- and 30-hour transfer times yielded acceptable outlet contours for these large tanks (arbitrarily defined as an outlet whose final radius is less than 1/5 the tank radius). In the 20-hour transfer mode with no static-pressure drop, the outlet diameters were 0.25 meter at approximately 2.05 meters from the origin of the hemispherical bottom in the liquid-oxygen tank and 0.404 meter at approximately 2.9 meters from the bottom in the liquid-hydrogen tank. The corresponding outlet diameters for a

static-pressure drop equal to the hydrostatic head were 0.210 meter in the liquid-oxygen tank and 0.338 meter in the liquid-hydrogen tank. In the 30-hour transfer mode with no static-pressure drop, the outlet diameters were 0.204 meter at 2.0 meter from the origin in the liquid-oxygen tank and 0.329 meter at 3.0 meter from the origin in the liquid-hydrogen tank. Again, corresponding outlet diameters with a static-pressure drop in the outlet were 0.172 meter in the liquid-oxygen tank and 0.272 meter in the liquid-hydrogen tank.

Should these tanks perform as anticipated, they could offer advantages over the systems discussed in reference 12. Operation could be simplified because no throttling or scavenging would be required since residuals would be drastically reduced or eliminated. Overall tank lengths could be reduced since less propellant could be carried because there would be a little or no residuals. Additionally, there appears to be an advantage in permitting a static-pressure drop in the outlet since this results in a smaller diameter outlet at any given axial position than would be the case with no static-pressure drop. In the cases considered here, the outlet diameters appear to be reduced by about 20 percent. This would substantially reduce the weight of the outlet region.

CONCLUSIONS

An analysis is presented and the developed equations solved to define the contour of a tank outlet that would prevent premature vapor ingestion during tank draining. The effects of surface tension have been neglected in the analysis, and thus the analysis is strictly true only for a flat interface. The effects of various system parameters were evaluated numerically and the following conclusions were drawn:

1. A 10:1 variation in liquid kinematic viscosity had only a minimal effect on the calculated outlet contour.
2. A 62.5:1 variation in gravity level (from 0.5 g to 0.008 g) had a significant effect on the calculated outlet contour. Furthermore, as the effective gravitational environment was reduced toward zero, the contoured-outlet size approached the tank size.
3. Increasing the outflow rate 4 times also had a significant effect on the calculated outlet contour, with the outlet-contour radius increasing with increasing outflow rate.

So that the draining performance of the contoured tank could be evaluated, some tanks were fabricated according to the equations presented for constant static pressure in the outlet line. When the tanks were drained at design conditions, the photographic data indicated that nearly all liquid was drained from the tanks. However, a small amount of liquid did adhere to the tank walls. This quantity of liquid was generally quite small and only became visible when the experiment package was decelerated at the conclusion of the test. Calculations indicated that approximately 5 milliliters of liquid remained in the 2-centimeter-radius tank when vapor was ingested and about 6 milliliters

in the 3-centimeter-radius tank. These amounts were considerably less than would be expected in a hemispherical-bottomed tank with a conventional outlet. Residuals were reduced 40 to 60 percent by the contouring.

When the tanks were drained at off-design conditions (i.e., when the test liquids were either trichlorotrifluoroethane or 60 percent ethanol and 40 percent glycerol, the effective gravitational environment was less than 0.015 g, and the outflow rate was greater than $20 \text{ cm}^3/\text{sec}$ for the smaller tank or $30 \text{ cm}^3/\text{sec}$ for the larger tank), the following qualitative observations were made:

4. The calculated liquid residuals increased slightly as the liquid viscosity increased when draining was performed at the design outflow rate and gravity level. A 35:1 increase in liquid kinematic viscosity gave rise to an 18 percent increase in liquid residuals in the larger tank and to a 16 percent increase in liquid residuals in the smaller tank. This was attributed primarily to a thicker boundary layer at the wall for the more viscous fluid.

5. For a given test liquid, decreasing the gravitational environment at a constant outflow rate increased the calculated liquid residuals.

6. For a given test liquid, increasing the outflow rate at a constant gravitational environment increased the calculated liquid residuals.

7. In all tests, the calculated liquid residuals for the contoured-outlet tank were lower than would have occurred for a tank with a constant-diameter outlet.

The contour equations were applied to two systems for space tug resupply, and the appropriate outlet contouring was obtained both for constant static pressure in the outlet and for a static-pressure drop equal to the hydrostatic head. The results indicated that the tank outlets converged to a final radius of less than 1/5 the tank radius at about 1 tank diameter from the origin of the original hemispherical bottom, with one exception. As expected, permitting some static-pressure drop to occur in the outlet resulted in a smaller outlet diameter at any given axial position than would have occurred were the static pressure held constant.

In conclusion, contouring the outlet line in accordance with the equations presented appears to be an attractive method for reducing or eliminating liquid residuals when a tank is drained in a low-gravity environment. Further, it is the opinion of the author that the wall liquid-layer thickness would not be substantially greater in larger tanks, and hence the magnitude of the dimensionless liquid residuals obtained in those tanks would be significantly less with outlet contouring than in a conventional-outlet tank.

Lewis Research Center,
National Aeronautics and Space Administration,
Cleveland, Ohio, April 25, 1979,
506-21.

APPENDIX A

DEVELOPMENT OF CONTOURED-OUTLET ANALYSIS

Vapor ingestion caused by suction dip into the outlet line during outflow from a tank will not occur if the draining liquid remains in its equilibrium configuration (as determined by the Bond number, the tank shape, and the contact angle) as it passes into and through the outlet line. In general, this objective could be achieved if the axial component of the velocity had no radial dependence at any fixed axial position in the tank or outlet. To achieve this objective, we seek an appropriate contour or shaping of the tank outlet line. A general outlet configuration (including a portion of the tank) is shown in figure 1 along with pertinent variables. The approach used herein is similar to that used in reference 9 and neglects the effects of surface tension.

If the liquid to be drained is incompressible and only conservative body forces due to gravitational acceleration act on the liquid, the extended Bernoulli equation between a point on the liquid-vapor interface and a point in the tank outlet region adjacent to the wall (including the viscous loss term due to the wall) is

$$\frac{1}{2} v_s^2 + \frac{P}{\rho} - (a + g)h - F = \text{Constant} \quad (A1)$$

We assume cylindrical coordinates, noting that there is symmetry in the θ -direction and that, in general, v_s , P , and F are functions of h and r . To find the outlet contour, we must first determine the outlet-contour radius r as a function of axial length h . This can be done by taking the total derivative of equation (A1) with respect to r to yield

$$\frac{1}{2} \frac{d}{dr} (v_s^2) + \frac{1}{\rho} \frac{dP}{dr} - (a + g) \frac{dh}{dr} - \frac{dF}{dr} = 0 \quad (A2)$$

Consider figure 1 and note that the axial velocity v_h can be expressed in terms of the streamline velocity v_s .

$$\left. \begin{aligned} v_h &= v_s \sin \alpha = v_s \frac{dh}{ds} \\ v_s &= \frac{ds}{dh} v_h \end{aligned} \right\} \quad (A3)$$

or

We now apply the specific requirement that the axial component of the velocity be uniform at each axial location and equal to the average velocity at that location

$$v_h = \frac{Q}{\pi r^2} \quad (A4)$$

Combining equations (A3) and (A4) gives the velocity in the bounding streamline

$$v_s = \frac{ds}{dh} \frac{Q}{\pi r^2} \quad (A5)$$

However, from figure 1,

$$ds = [(dh)^2 + (-dr)^2]^{1/2} = [(dh)^2 + (dr)^2]^{1/2}$$

and

$$\frac{ds}{dh} = \left[1 + \left(\frac{dr}{dh} \right)^2 \right]^{1/2} = \left[1 + \left(\frac{dh}{dr} \right)^{-2} \right]^{1/2}$$

Thus equation (A5) can be rewritten as

$$v_s = \frac{Q}{\pi r^2} \left[1 + \left(\frac{dh}{dr} \right)^{-2} \right]^{1/2} \quad (A6)$$

and

$$(v_s)^2 = \frac{Q^2}{\pi^2 r^4} \left[1 + \left(\frac{dh}{dr} \right)^{-2} \right] \quad (A7)$$

Taking the derivative of equation (A7) with respect to the radius r gives

$$\frac{d}{dr} (v_s^2) = \frac{-2Q^2}{\pi^2 r^4} \left\{ \left(\frac{dh}{dr} \right)^{-3} \left(\frac{d^2 h}{dr^2} \right) + \frac{2}{r} \left[1 + \left(\frac{dh}{dr} \right)^{-2} \right] \right\} \quad (A8)$$

We can approximate the incremental head loss df along the contour by assuming that the chosen differential element is cylindrical (fig. 1) and using the Darcy-Weisbach equation for pipe flow:

$$dF = \frac{f}{D} (dS) \frac{v_s^2}{2} = \frac{f}{2r} (dS) \frac{v_s^2}{2}$$

and

$$\frac{dF}{dr} = \frac{f}{4r} \left(\frac{dS}{dr} \right) v_s^2 \quad (A9)$$

but

$$\frac{dS}{dr} = \left[1 + \left(\frac{dh}{dr} \right)^2 \right]^{1/2} \quad (A10)$$

By substituting equations (A7) to (A10) into the differential form of the Bernoulli equation (A12) and letting $G \equiv (a + g)$, that is, the total acceleration, we obtain

$$\frac{-Q^2}{\pi^2 r^4} \left\{ \left(\frac{dh}{dr} \right)^{-3} \left(\frac{d^2 h}{dr^2} \right) + \frac{2}{r} \left[1 + \left(\frac{dh}{dr} \right)^{-2} \right] \right\} + \frac{1}{\rho} \frac{dP}{dr} - G \frac{dh}{dr} - \frac{f}{4\pi^2} \frac{Q^2}{r^5} \left[1 + \left(\frac{dh}{dr} \right)^{-2} \right] \left[1 + \left(\frac{dh}{dr} \right)^2 \right]^{1/2} = 0 \quad (A11)$$

The coefficient of the d^2h/dr^2 term can be made equal to unity by multiplying the entire expression through by

$$\frac{-\pi^2 r^4}{Q^2} \left(\frac{dh}{dr} \right)^3$$

to yield

$$\frac{2}{r} \left(\frac{dh}{dr} \right)^3 + \frac{2}{r} \left(\frac{dh}{dr} \right) + \frac{d^2 h}{dr^2} + \frac{G\pi^2 r^4}{Q^2} \left(\frac{dh}{dr} \right)^4 - \frac{\pi^2 r^4}{Q^2 \rho} \left(\frac{dh}{dr} \right)^3 \left(\frac{dP}{dr} \right) + \frac{f}{4r} \left(\frac{dh}{dr} \right)^3 \left[1 + \left(\frac{dh}{dr} \right)^{-2} \right] \left[1 + \left(\frac{dh}{dr} \right)^2 \right]^{1/2} = 0 \quad (A12)$$

Constant Static Pressure

We first assume that the static pressure remains constant or equivalently that dP/dr in equation (A12) is zero. This condition would be desirable when the tank pressure is initially quite close to the vapor pressure of the liquid and any attendant de-

crease in static pressure would cause cavitation in the outlet line. This assumption necessarily leads to predicting both a longer and wider outlet line than would be predicted if some static-pressure drop were permitted. However, it has the advantage of providing vapor-free outflow for a wider range of liquid flows and pressures.

For this case, equation (A12) can be written as

$$\frac{d^2h}{dr^2} + \frac{2}{r} \left[\left(\frac{dh}{dr} \right)^3 + \left(\frac{dh}{dr} \right) \right] + \frac{f}{4r} \left(\frac{dh}{dr} \right)^3 \left[1 + \left(\frac{dh}{dr} \right)^{-2} \right] \left[1 + \left(\frac{dh}{dr} \right)^2 \right]^{1/2} + \left(\frac{dh}{dr} \right)^4 \left(\frac{G\pi^2 r^4}{Q^2} \right) = 0$$

or

$$\frac{d^2h}{dr^2} + \frac{2}{r} \left(\frac{dh}{dr} \right)^3 \left[1 + \left(\frac{dh}{dr} \right)^{-2} \right] + \frac{f}{4r} \left(\frac{dh}{dr} \right)^3 \left[1 + \left(\frac{dh}{dr} \right)^{-2} \right] \left[1 + \left(\frac{dh}{dr} \right)^2 \right]^{1/2} + \left(\frac{dh}{dr} \right)^4 \left(\frac{G\pi^2 r^4}{Q^2} \right) = 0$$

which reduces to

$$\frac{d^2h}{dr^2} + \frac{2}{r} \left(\frac{dh}{dr} \right) \left[1 + \left(\frac{dh}{dr} \right)^2 \right] \left\{ 1 + \frac{f}{8} \left[1 + \left(\frac{dh}{dr} \right)^2 \right]^{1/2} \right\} + \left(\frac{dh}{dr} \right)^4 \left(\frac{G\pi^2 r^4}{Q^2} \right) = 0 \quad (A13)$$

From figure 1, $-dh/dr = T = \text{Slope}$. There equation (A13) can be written as

$$\frac{dT}{dr} + \frac{2T}{r} (1 + T^2) \left[1 + \frac{f}{8} (1 + T^2)^{1/2} \right] - T^4 \left(\frac{G\pi^2 r^4}{Q^2} \right) = 0 \quad (A14)$$

With the method of reference 9, we can solve the constant-static-pressure equation (A14) numerically by assuming that the typical contoured outlet consists of a large number of frustums of cones with equal (dh/dr) to the negative of the slope of each conical segment (fig. 2). Further, since the slope of any conical segment is constant, $dT/dr = 0$ and equation (A14) becomes

$$\frac{2T}{r} (1 + T^2) \left(1 + \frac{f}{8} \sqrt{1 + T^2} \right) - \frac{T^4 G r^4 \pi^2}{Q^2} = 0 \quad (A15)$$

and is valid for each frustum. For laminar flow, the friction factor f can be given as $64/Re$. Therefore

$$f = \frac{32\mu\pi r}{\rho Q} \quad (A16)$$

In general, as the flow enters the tank outlet, it is laminar and could conceivably undergo transition to turbulent flow. However, for this analysis the laminar-flow friction factor (eq. (A16)) is used. Substituting equation (A16) into (A15) yields

$$\frac{2T}{r} (1 + T^2) \left(1 + \frac{4\mu\pi r}{\rho Q} \sqrt{1 + T^2} \right) = T^4 \frac{Gr^4 \pi^2}{Q^2}$$

or, after rearranging,

$$r^5 = \frac{2Q^2}{T^3 G \pi^2} (1 + T^2) \left(1 + \frac{4\mu\pi r}{\rho Q} \sqrt{1 + T^2} \right) \quad (A17)$$

If we let

$$A_1 = \frac{2Q^2}{\pi^2}$$

and

$$B_1 = \frac{4\mu\pi}{\rho Q}$$

equation (A17) can be written as

$$r^5 = \frac{A_1}{T^3 G} (1 + T^2) \left(1 + B_1 r \sqrt{1 + T^2} \right) \quad (A18)$$

Equation (A18) is then the governing equation that, when solved, defines the appropriate outlet contour. The method of solution is to choose r equal to the tank radius and solve equation (A18) to determine an initial value of the slope T . Then by using an incremental change to T (e.g., 0.1), the corresponding new radii are determined. Each calculated radius is assumed to occur at the midpoint of each conical frustum (see middle dashed line in fig. 2). The height difference between successive radii can be obtained from the product of the average slope and the radius difference

$$\Delta h = \frac{(r_1 - r_2)(T_2 + T_1)}{2} \quad (A19)$$

or, in more general form, from

$$h_n = h_{n-1} + \frac{(r_{n-1} - r_n)(T_n + T_{n-1})}{2} \quad (A20)$$

Equation (A20) is in the same form as equation (67) in reference 9.

Static-Pressure Drop

We now consider the case where the static pressure drops as flow passes into and through the outlet. This results in a slightly narrower outlet than for no static-pressure drop. We can begin from equation (A12), which is rewritten as

$$\frac{d^2h}{dr^2} + \frac{2}{r} \left(\frac{dh}{dr} \right) \left[1 + \left(\frac{dh}{dr} \right)^2 \right] \left\{ 1 + \frac{f}{8} \left[1 + \left(\frac{dh}{dr} \right)^2 \right]^{1/2} \right\} + \frac{\pi r^4}{Q^2} \left(\frac{dh}{dr} \right)^3 \left[G \frac{dh}{dr} - \frac{1}{\rho} \frac{dP}{dr} \right] = 0 \quad (A21)$$

Again, we note from figure 1 that $-dh/dr = T = \text{Slope}$ and rewrite equation (A21) as

$$\frac{-dT}{dr} - \frac{2T}{r} (1 + T^2) \left[1 + \frac{f}{8} (1 + T^2)^{1/2} \right] - \frac{\pi^2 r^4}{Q^2} T^3 \left(-GT - \frac{1}{\rho} \frac{dP}{dr} \right) = 0 \quad (A22)$$

As before, we assume that the outlet consists of a large number of frustums of cones with dh/dr equal to the negative of the slope of each conical segment (fig. 2). Further, since the slope of any conical segment is constant, $dT/dr = 0$ and equation (A22) becomes

$$\frac{2T}{r} (1 + T^2) \left[1 + \frac{f}{8} (1 + T^2)^{1/2} \right] + \frac{\pi^2 r^4}{Q^2} T^3 \left(-GT - \frac{1}{\rho} \frac{dP}{dr} \right) = 0 \quad (A23)$$

and is valid for each frustum. Solving equation (A23) for r yields

$$r^5 = \frac{2Q^2}{\pi^2} \frac{(1 + T^2) \left(1 + \frac{f}{8} \sqrt{1 + T^2} \right)}{T^2 \left[GT + \frac{1}{\rho} \left(\frac{dP}{dr} \right) \right]} \quad (A24)$$

Since, in general, $P = P(h, r)$,

$$\left. \begin{aligned} \frac{dP}{dr} &= \left(\frac{\partial P}{\partial h} \right) \left(\frac{dh}{dr} \right) + \left(\frac{\partial P}{\partial r} \right) \left(\frac{dr}{dr} \right) \\ \frac{dP}{dr} &= \frac{\partial P}{\partial r} - T \frac{\partial P}{\partial h} \end{aligned} \right\} \quad (A25)$$

or

Since we have already assumed that the flow is uniform at any cross section in the outlet, letting $\partial P / \partial r = 0$ changes equation (A25) to

$$\frac{dP}{dr} = -T \frac{\partial P}{\partial h} \quad (A26)$$

We now must determine $\partial P / \partial h$. If the axial pressure drop is equal to the rise in the hydrostatic pressure (i.e., $P = -\rho Gh + P_0$),

$$\frac{\partial P}{\partial h} = -\rho G \quad (A27)$$

Substituting equation (A27) into (A26) gives

$$\frac{dP}{dr} = \rho GT \quad (A28)$$

Thus equation (A24) becomes

$$r^5 = \frac{2Q^2}{\pi^2} \frac{(1 + T^2) \left(1 + \frac{f}{8} \sqrt{1 + T^2} \right)}{2GT^3} \quad (A29)$$

As before, we assume laminar flow with the friction factor f being given as

$$f = \frac{64}{Re} = \frac{32\mu\pi r}{\rho Q}$$

and

$$A_1 = \frac{2Q^2}{\pi^2}$$

and

$$B_1 = \frac{4\mu\pi}{\rho Q}$$

Therefore equation (A29) becomes

$$r^5 = \frac{A_1(1 + T^2) \left(1 + B_1 r \sqrt{1 + T^2}\right)}{2GT^3} \quad (A30)$$

Equation (A30) is then the governing equation that, when solved, defines the appropriate outlet contour when a static-pressure drop equal to the hydrostatic head is permitted in the outlet. Equation (A30) is very similar in form to equation (A18), and the method of solution is exactly the same. This result differs from the result of reference 9, in which it was assumed that

$$\frac{\partial P}{\partial h} \equiv \rho G \frac{dh}{dr}$$

APPENDIX B

APPARATUS AND PROCEDURE

Facility

The experiment data for this study were obtained in the Zero Gravity Facility at the Lewis Research Center. A schematic drawing of the facility is shown in figure 12. The facility consists of a concrete-lined, 8.5-meter-diameter shaft that extends 155 meters below ground level. A steel vacuum chamber, 6.1 meters in diameter and 143 meters high, is contained within the concrete shaft. The pressure in this vacuum chamber is reduced to 13.3 N/m^2 by using the Center's wind-tunnel exhaust system and an exhaust-er system located within the facility.

The ground-level service building has as its major components a shop area, a control room, and a clean room. Assembly, servicing, and balancing of the experiment vehicle are done in the shop area. Tests are conducted from the control room, shown in figure 13, which contains the exhauster control system, the experiment-vehicle predrop checkout and control system, and the data retrieval system. Those components of the experiment that contact the test fluid are prepared in the facility's class-10 000 clean room, shown in figure 14. The major elements in this room are an ultrasonic cleaning system (fig. 14(a)) and a class-100 laminar flow station (fig. 14(b)) for preparing those experiments requiring more than normal cleanliness.

Operating. - The Zero Gravity Facility allows the experiment vehicle to fall freely from the top of the vacuum chamber, for nominally 5 seconds of free-fall time. The experiment vehicle falls freely; that is, no guide wires, electrical lines, and so forth, are connected to the vehicle. Therefore, the only force (aside from gravity) acting on the freely falling experiment vehicle is residual air drag. This results in an equivalent gravitational acceleration acting on the experiment that is estimated to be about 10^{-5} g maximum.

Recovery system. - After the experiment vehicle has traversed the total length of the vacuum chamber, it is decelerated in a 3.6-meter-diameter, 6.1-meter-deep container that is located on the vertical axis of the chamber and is filled with small pellets of expanded polystyrene. The deceleration rate, averaging about 35 g's, is controlled by the flow of these pellets in the annular area between the experiment vehicle and the wall of the deceleration container. The decelerator container mounted on the cart is shown in figure 15.

Experiment Vehicle

The experiment vehicle used to obtain the data for this study is shown in figure 16. The vehicle consists of a telemetry section (contained in the top fairing), an experiment section (contained in the cylindrical midsection) and a thrust system (contained in the conical base).

Telemetry section. - The on-board telemetry system used to collect and transmit data is a standard Inter-Range Instrumentation Group (IRIG) FM/FM 2200-megahertz telemeter. It records as many as 18 channels of continuous data during a test drop. The system frequency range extends to 2100 hertz. The telemetered data are recorded on two high-response recording oscilloscopes located in the control room.

Experiment section. - The experiment section, shown in figure 17, is a self-contained unit consisting of an experiment tank, a pumping or liquid flow system, a photographic and lighting system, a digital clock, and an electrical system to operate the various components. An air reservoir, the experiment tank, an orifice, a solenoid valve, a flowmeter, and a collection tank are connected to form the liquid flow system. Indirect illumination of the experiment tank provides enough light for the behavior of the liquid-vapor interface during draining to be recorded with a high-speed, 16-millimeter motion-picture camera. A clock with a calibrated accuracy of 0.01 second is positioned within the camera's field of view to indicate the elapsed time during the drop. The electrical components on board the package are operated through a control box and receive their power from rechargeable nickel-cadmium cells.

Thrust system. - The conical base of the experiment vehicle contains the cold-gas thrust system and can produce thrusts from 13 to 130 newtons for 5 seconds or longer. The acceleration was calculated from the calibrated thrust and the package weight. Before the thrust system was installed on the experiment vehicle, it was calibrated on a static thrust-calibration stand located in the facility vacuum chamber. This calibration was done at pressure levels corresponding to test drop conditions. A null-balance, load-cell system was used to record the thrust-time history as a function of thrust-nozzle inlet pressure and size.

Test Procedure

The test containers were cleaned ultrasonically before each test in the facility's clean room (fig. 14). The cleaning consisted of ultrasonic immersion in a solution of detergent and water, rinsing with a solution of distilled water and methanol, and drying in a warm-air dryer.

The containers were then mounted on the experiment package, and liquid was added to fill the test tank to the desired fill level. Pressure was added to the accumulator

bottles and a normal-gravity test was made to set the proper flow rate. The volume of air in the reservoir was sufficiently large in comparison with the volume of the displaced liquid that the change in pressure in the experiment tank was negligible during a test.

During a drop, a predetermined time increment was allowed so that the interface could reach its low point in the first pass through its equilibrium configuration. At this time, outflow was begun and continued until vapor was ingested into the tank outlet. Electrical timers carried on board the experiment vehicle were adjusted to control the start as well as the duration of these functions on a drop. The experiment vehicle was balanced about its vertical axis to ensure accurate drop trajectory and thrust alignment with respect to the experiment tank. Accurate thrust alignment is essential to provide an axisymmetric, equilibrium liquid-vapor interface shape.

After all predrop functions were properly set, the experiment vehicle was positioned at the top of the vacuum chamber as shown in figure 18. It was suspended by the support shaft on a hinged-plate release mechanism. During vacuum-chamber pumpdown and before release, the experiment vehicle system was monitored through an umbilical cable attached to the top of the support shaft. Electrical power was supplied by ground equipment. The system was then switched to internal power a few minutes before release. The umbilical cable was remotely pulled from the support shaft 0.5 second before package release and the thrust system (when used) was activated 0.2 second before release to allow the thrust to reach steady-state conditions. The vehicle was released by pneumatically shearing a bolt that holds the hinged plate in the closed position. No measurable disturbances were imparted to the experiment by this release system.

The total free-fall test time obtained in this mode was 5.16 seconds. Approximately 0.13 second before the experiment package entered the deceleration cart, the thrust system was shut down to avoid dispersing the deceleration material. During the test, the vehicle's trajectory and deceleration were monitored on closed-circuit television. After the test drop, the vacuum chamber was vented to the atmosphere and the experiment vehicle was returned to ground level.

REFERENCES

1. Derdul, Joseph D.; Grubb, Lynn S.; and Pettrash, Donald A.: Experimental Investigation of Liquid Outflow from Cylindrical Tanks during Weightlessness. NASA TN D-3746, 1966.
2. Berenyi, Steven G.; and Abdalla, Kaleel L.: The Liquid-Vapor Interface during Outflow in Weightlessness. NASA TM X-1811, 1969.
3. Abdalla, Kaleel, L.; and Berenyi, Steven G.: Vapor Ingestion Phenomenon in Weightlessness. NASA TN D-5210, 1969.
4. Berenyi, Steven G.; and Abdalla, Kaleel L.: Vapor Ingestion Phenomenon in Hemispherically Bottomed Tanks in Normal Gravity and in Weightlessness. NASA TN D-5704, 1970.
5. Berenyi, Steven G.: Effect of Outlet Baffling on Liquid Residuals for Outflow from Cylinders in Weightlessness. NASA TM X-2018, 1970.
6. Symons, Eugene P.: Outlet Baffles - Effect on Liquid Residuals from Zero Gravity Draining of Hemispherically Ended Cylinders. NASA TM X-2631, 1972.
7. Symons, Eugene P.: Effect of Throttling on Interface Behavior and Liquid Residuals in Weightlessness. NASA TM X-3034, 1974.
8. Morey, T. F.; and Mason, G. E.: Tank Outlet Design for Non-Newtonian Fluids. Transactions of the Eighth Symposium on Ballistic Missile and Space Technology, vol. 1, 1963, pp. 13-29.
9. Holle, Glenn F.: Propellant Tank Outlet Designs. TM-0441-69-07, Martin Marietta Corp., 1969.
10. Siegert, Clifford E.; Pettrash, Donald A.; and Otto, Edward W.: Time Response of Liquid-Vapor Interface after Entering Weightlessness. NASA TN D-2458, 1964.
11. Bizzell, G. D.; and Crane, G. E.: Numerical Simulation of Low Gravity Draining. (LMSC-D521581, Lockheed Missiles and Space Co.; NASA Contract NAS3-17798.) NASA CR-135004, 1976.
12. Stark, J. A.: Low-G Fluid Transfer Technology Study. (C ASD-NAS-76-014, General Dynamics/Convair; NASA Contract NAS3-17814.) NASA CR-134911, 1976.

TABLE I. - PROPERTIES OF TEST LIQUIDS

[Contact angle with cast acrylic plastic in air, 0° .]

Test liquid	Surface tension at 20° C , σ , dynes/cm	Density at 20° C , ρ , g/cm ³	Viscosity at 20° C , μ , g/(cm · sec)	Specific surface tension, β , cm ³ /sec ²
Ethanol	22.3	0.789	1.2	28.3
Trichlorotrifluoroethane	18.6	1.58	.7	11.8
60 Percent ethanol and 40 percent glycerol (percent by volume)	26.9	.988	15.4	27.2

TABLE II. - INTERFACE FORMATION TIMES

[Gravitational environment, 0.015 g.]

Tank radius, R_T , cm	Test liquid	Time to reach low point, sec
3	Trichlorotrifluoroethane	0.57
3	Ethanol	.40
3	60 Percent ethanol and	{ .41
2	40 percent glycerol	
2	Ethanol	.23
2	Trichlorotrifluoroethane	.20
		.35

TABLE III. - SUMMARY OF EXPERIMENT DATA

Test liquid	Tank radius, R_T , cm	Weber number, We , $Q^2/\pi^2\beta R_T^3$	Bond number, Bo , aR_T^2/β	Froude number, Fr , $Q^2/\pi^2 aR_T^5$	Calculated nondimensional residual, V	Approximate nondimensional residual without contouring, V (from refs. 4 and 11)
Ethanol	a_3	0.12	4.68	0.026	0.11 ± 0.05	0.28
	3	.12	2.19	.055	$.16 \pm 0.05$.37
		.12	0	∞	$.35 \pm 0.05$.60
		.48	4.68	.103	$.22 \pm 0.05$.50
		1.99	4.68	.425	$.65 \pm 0.05$.90
		8.46	4.68	1.81	$.98 \pm 0.05$	1.10
	a_2	.24	2.08	.115	$.30 \pm 0.075$.50
	2	.18	0	∞	$.40 \pm 0.075$.68
		1.14	2.08	.548	$.65 \pm 0.075$.85
		4.82	2.08	2.32	$.88 \pm 0.075$	1.10
		11.64	2.08	5.60	$.61 \pm 0.075$	1.20
Trichlorotrifluoroethane	3	0.28	11.23	0.0249	0 ± 0.05	0.30
	2	.43	4.99	.0861	$.16 \pm 0.075$.60
60 Percent ethanol and 40 percent glycerol	3	0.13	4.86	0.0267	0.18 ± 0.05	0.28
	2	.20	2.16	.0926	$.32 \pm 0.075$.48

^aDesign case.

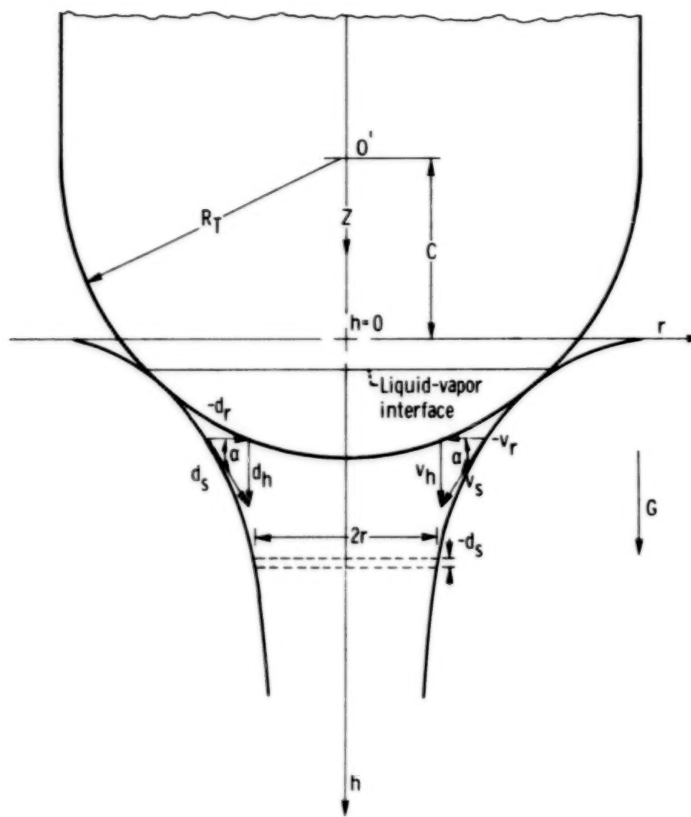


Figure 1. - General contoured-outlet configuration and variables.

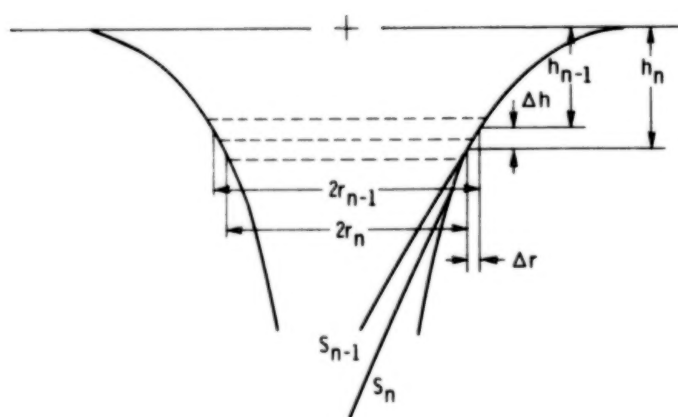


Figure 2. - Definition of terms - numerical scheme.

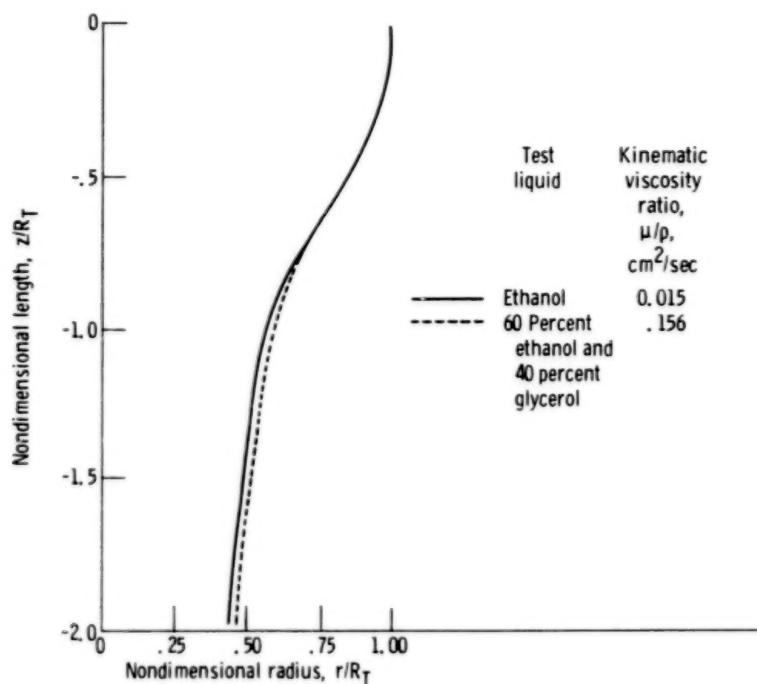


Figure 3. - Effect of viscosity on outlet contour for fixed flow rate and gravitational environment. Flow rate, 20 milliliters/sec; gravity level, 0.015 g; static pressure, constant.

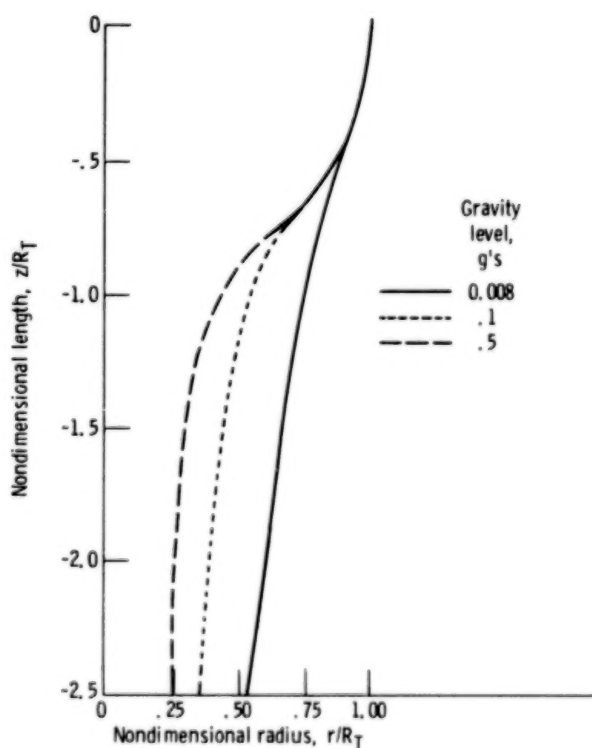


Figure 4. - Effect of gravitational environment on outlet contour for fixed outflow rate. Test liquid, ethanol; outflow rate, 20 milliliters/sec; static pressure, constant.

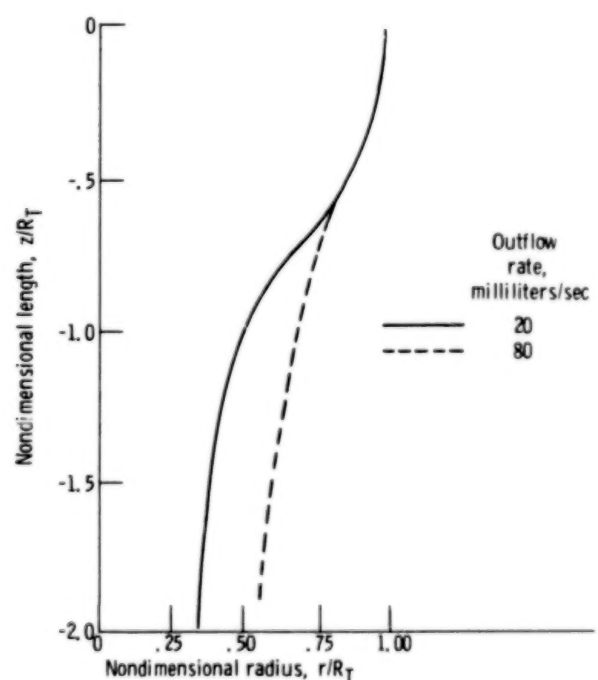


Figure 5. - Effect of outflow rate on outlet contour for fixed gravitational environment. Test liquid, ethanol; gravity level, 0.015 g; static pressure, constant.

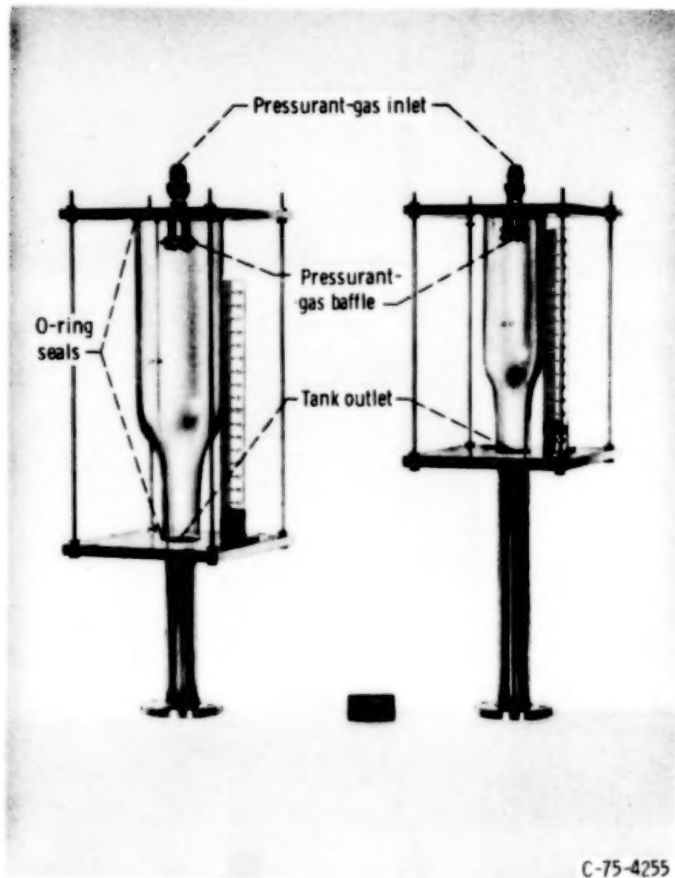
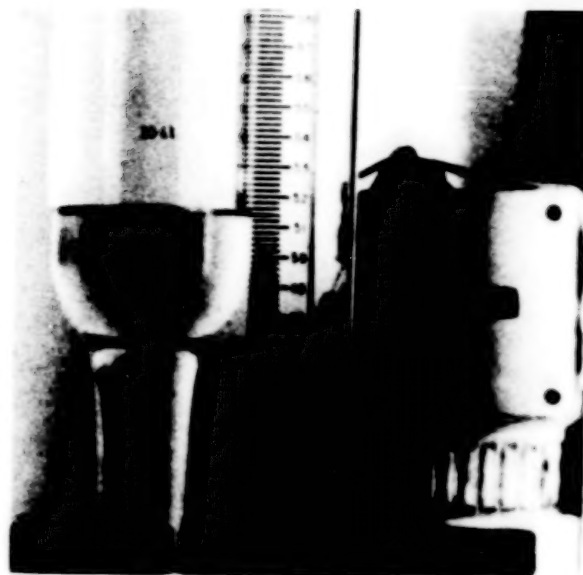
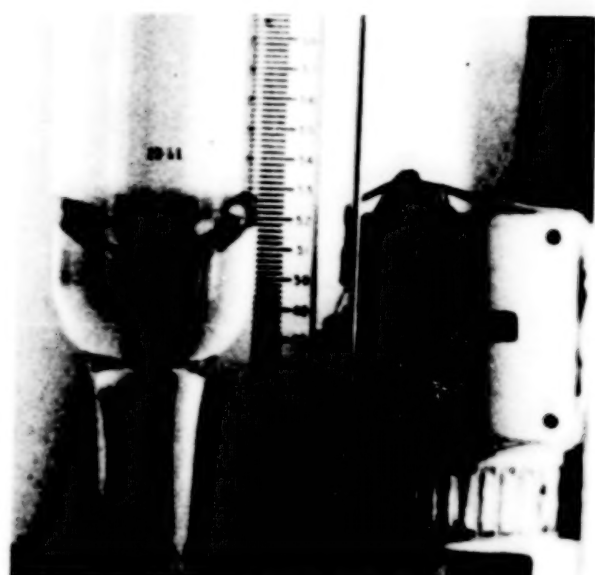


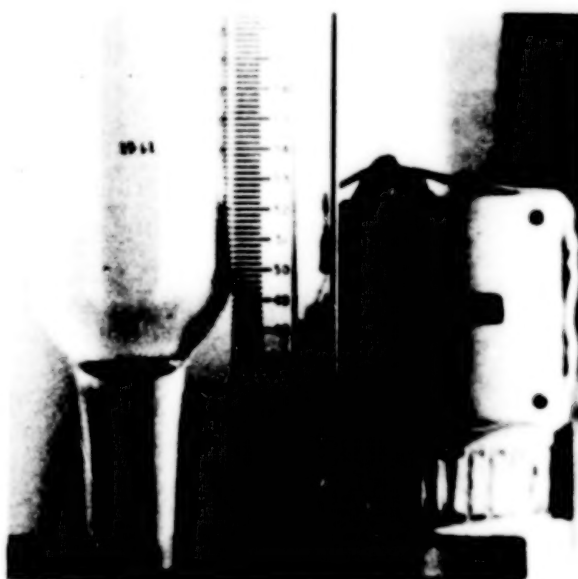
Figure 6. - Experiment tanks.



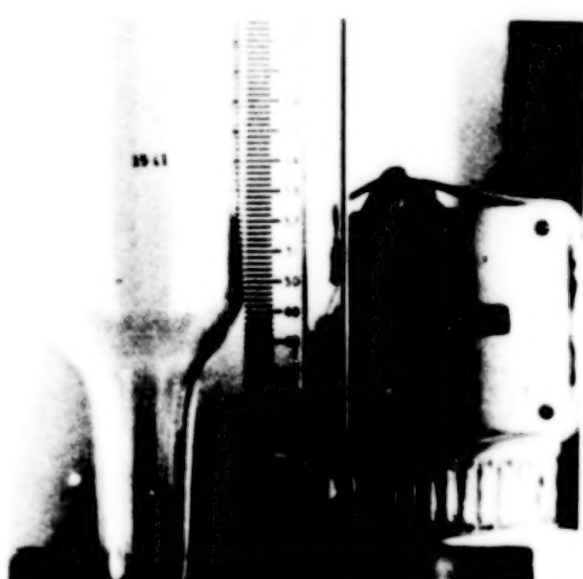
(a-1) In normal gravity.



(a-2) At start of draining.



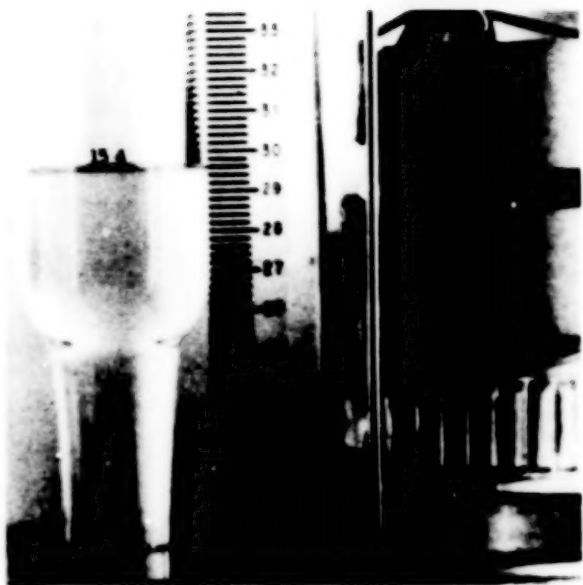
(a-3) At entrance to contoured section.



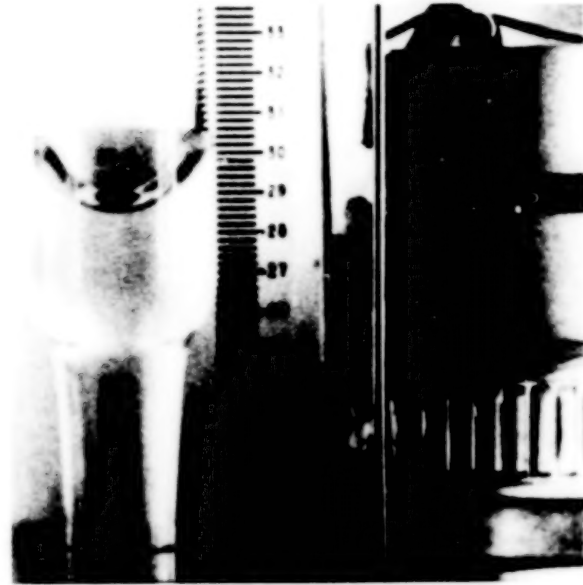
(a-4) At bottom of contoured section.

(a) Test liquid, ethanol; tank radius, 3 centimeters; Bond number, 4.68; Weber number, 0.125.

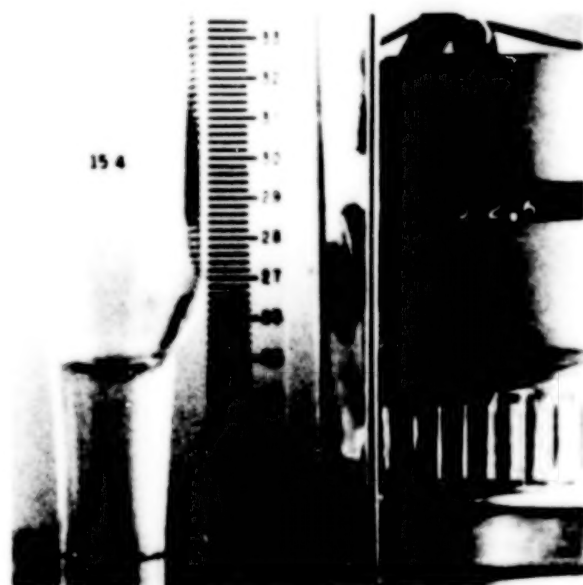
Figure 7. - Configuration of liquid-vapor interface during draining at design conditions.



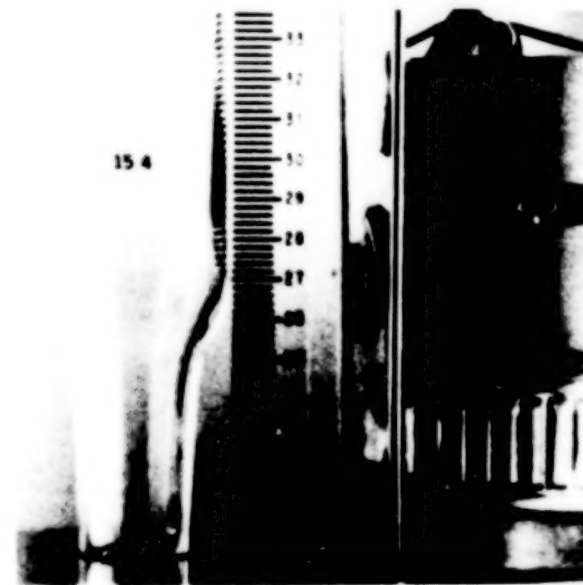
(b-1) In normal gravity.



(b-2) At start of draining.



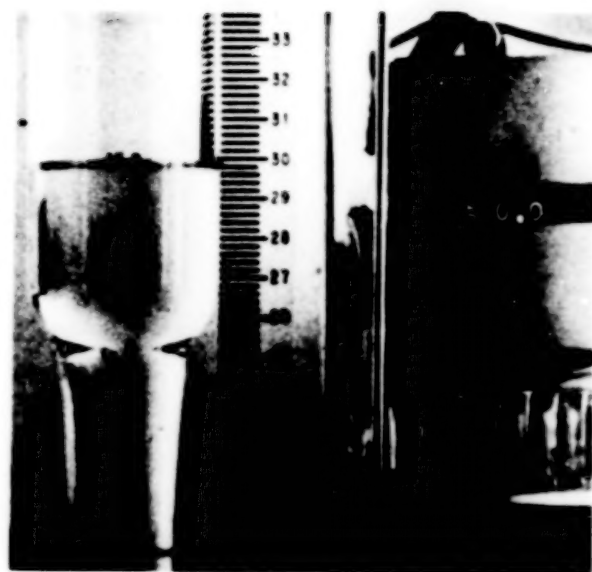
(b-3) At entrance to contoured section.



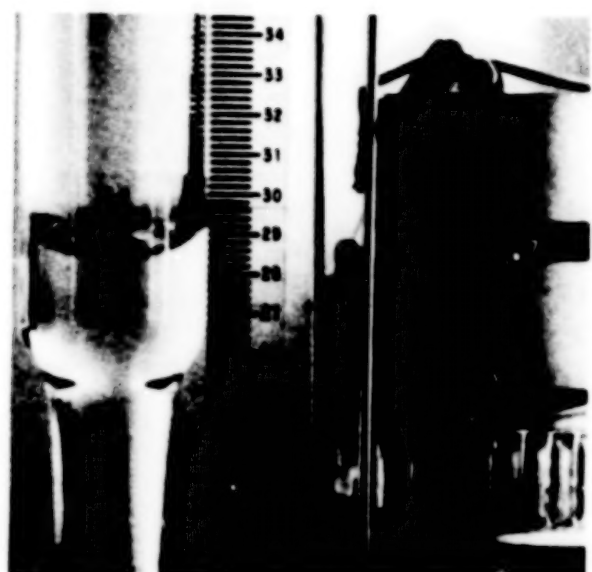
(b-4) At bottom of contoured section.

(b) Test liquid, ethanol; tank radius, 2 centimeters; Bond number, 2.08; Weber number, 0.177.

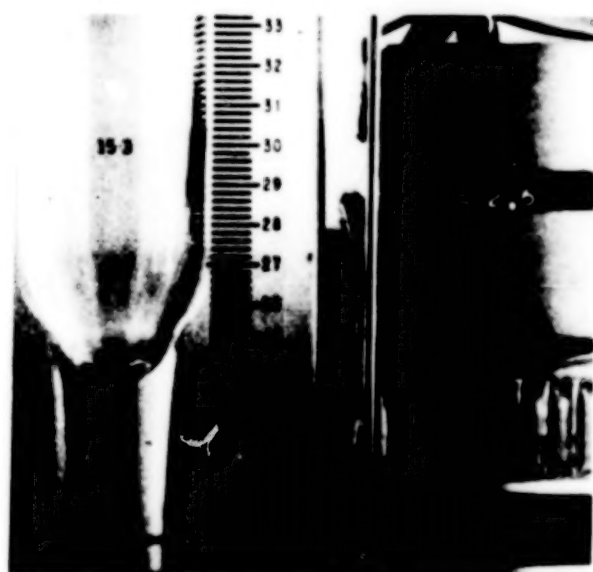
Figure 7. - Concluded.



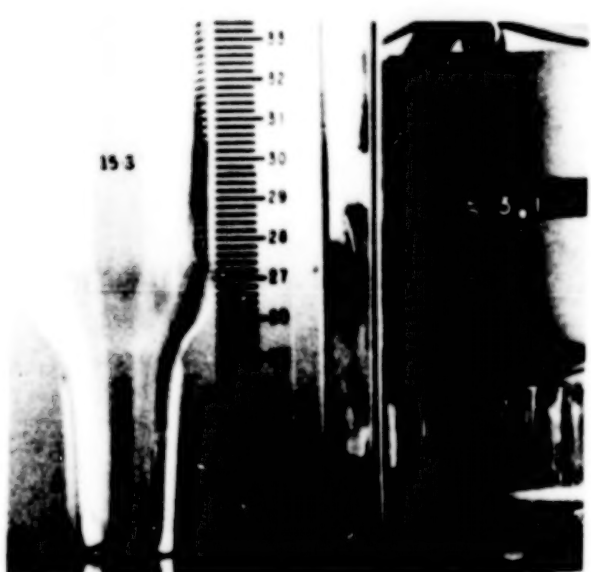
(a) In normal gravity.



(b) At start of draining.

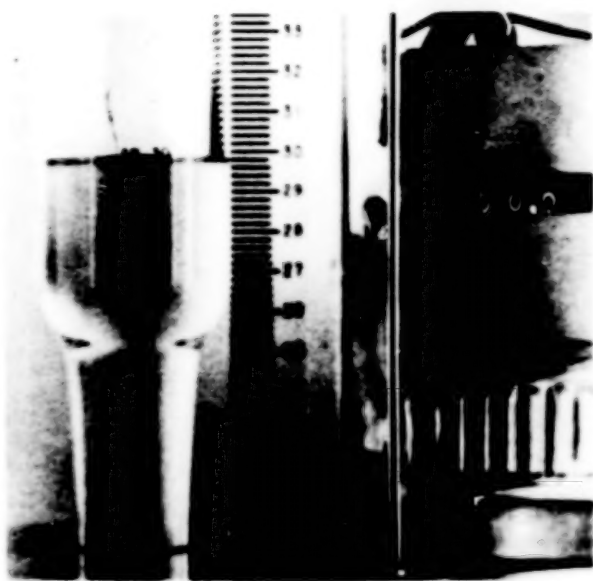


(c) At entrance to contoured section.

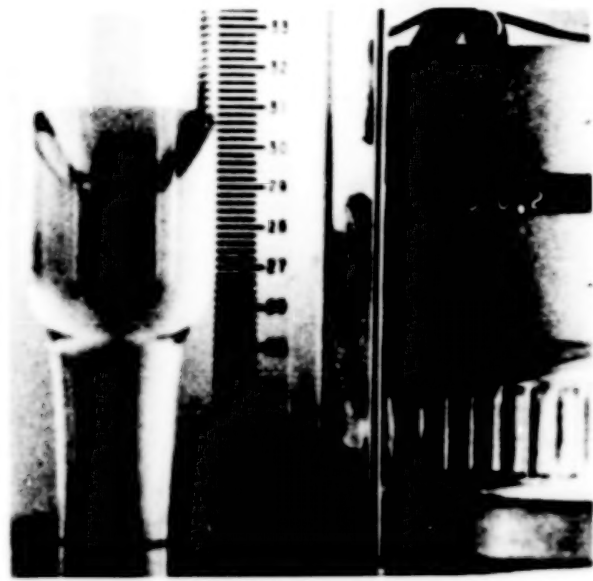


(d) At bottom of contoured section.

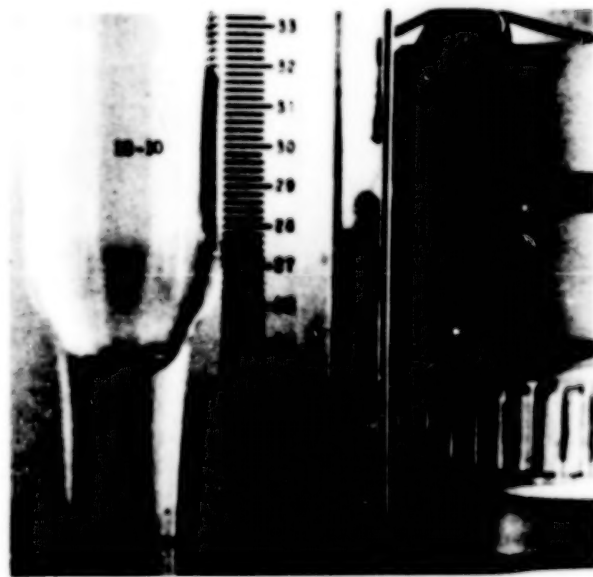
Figure 8. - Configuration of liquid-vapor interface during draining of a viscous liquid. Test liquid, 60 percent ethanol and 40 percent glycerol; tank radius, 2 centimeters; Bond number, 2.16; Weber number, 0.203.



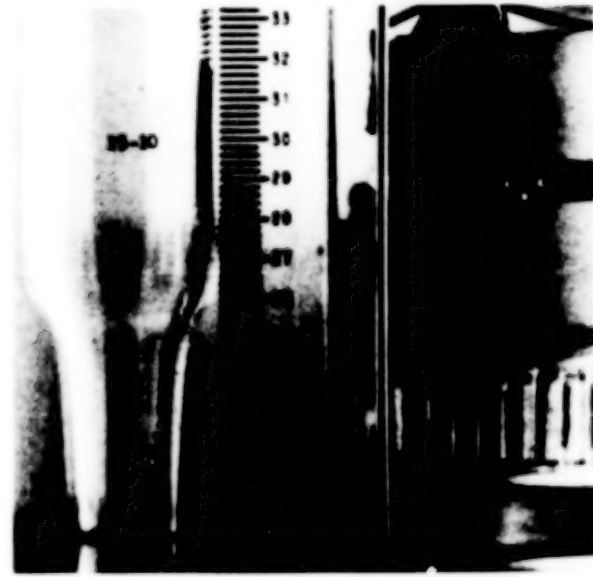
(a) In normal gravity.



(b) At start of draining.

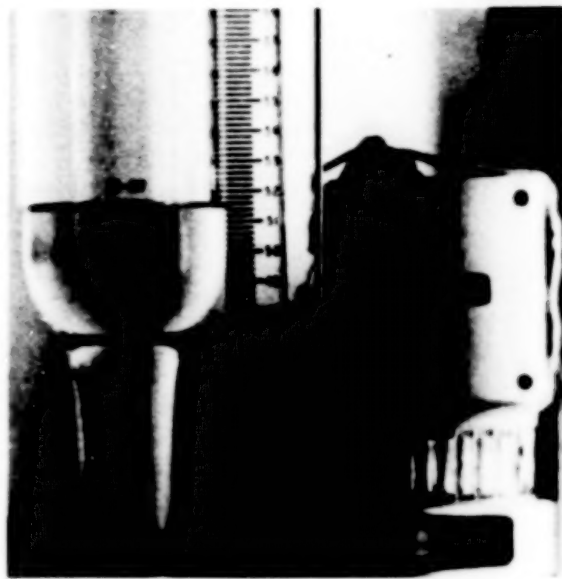


(c) At entrance to contoured section.

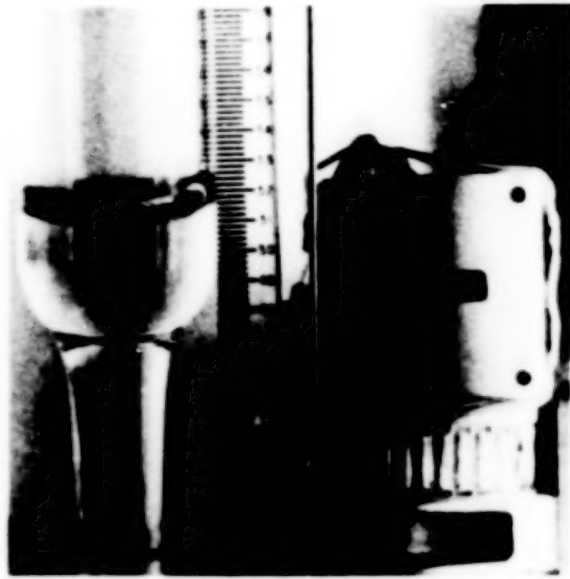


(d) At bottom of contoured section.

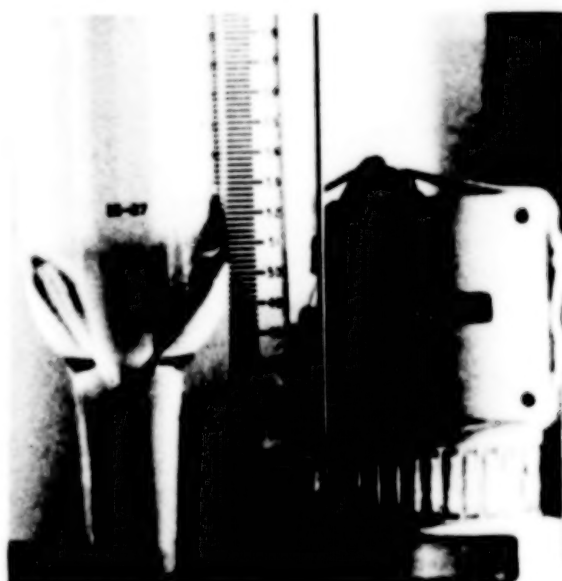
Figure 9. - Configuration of liquid-vapor interface during draining in weightlessness. Test liquid, ethanol; tank radius, 2 centimeters; Bond number, 0; Weber number, 0.182.



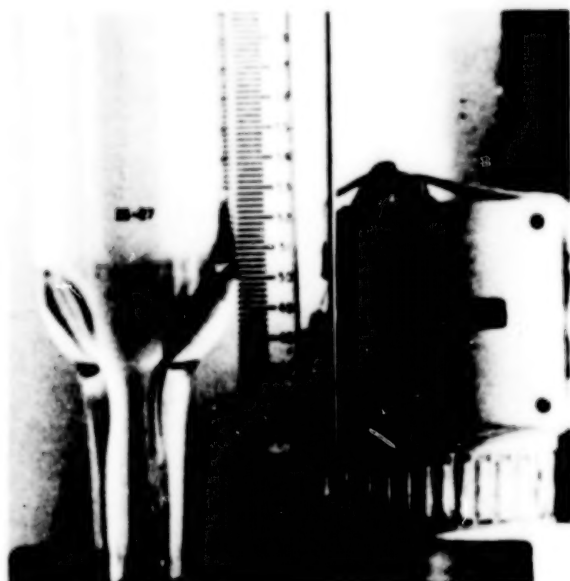
(a) In normal gravity.



(b) At start of draining.



(c) At entrance to contoured section.



(d) At bottom of contoured section.

Figure 10. - Configuration of liquid-vapor interface during draining at higher-than-design outflow rates. Test liquid, ethanol; tank radius, 3 centimeters; Bond number, 4.68; Weber number, 8.46.

System	Dimension, m					
	A	B	C	D	E	F
Separated from shuttle - constant static pressure	0.5	1.5	0.228	0.9	2.0	0.369
Separated from shuttle - static-pressure drop			.191	1.0		.309
Shuttle drag - constant static pressure; 10-hour transfer			.354	.8		.572
Shuttle drag - static-pressure drop; 10-hour transfer			.296	.9		.481
Shuttle drag - constant static pressure; 20-hour transfer	.55		.250	.95		.404
Shuttle drag - static-pressure drop; 20-hour transfer	.6		.210	1.0		.338
Shuttle drag - constant static pressure; 30-hour transfer	.5		.204	1.0		.329
Shuttle drag - static-pressure drop; 30-hour transfer	.6		.172	1.0		.272

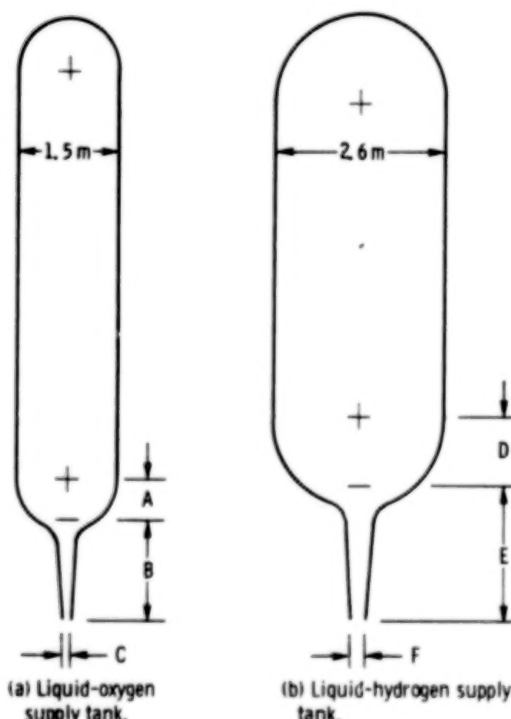


Figure 11. - Contoured-outlet tanks for space tug in-orbit supply system.

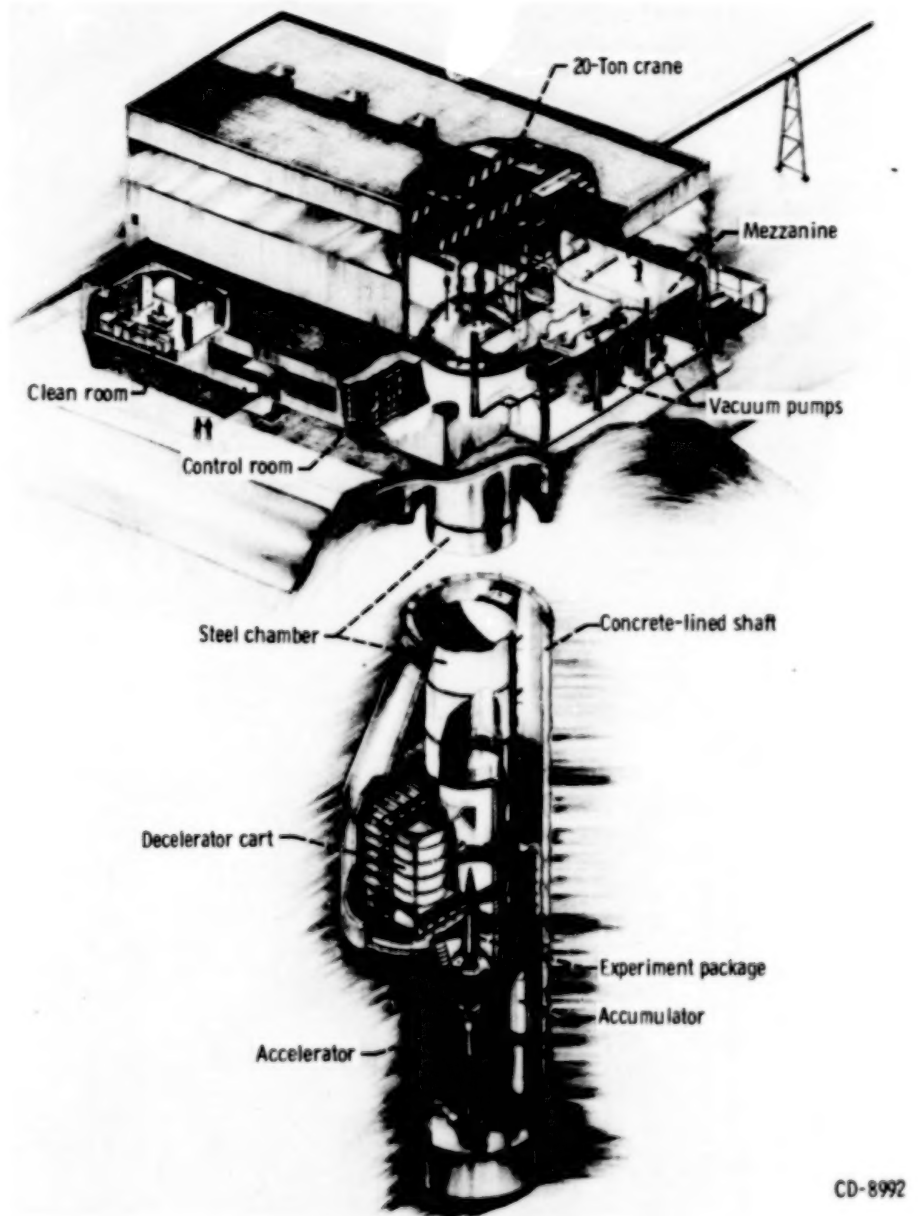


Figure 12. - Illustration of 5- to 10-Second Zero-Gravity Facility.



C-67-2568

Figure 13. - Control room.



(a) Ultrasonic cleaning system.



(b) Laminar-flow work station.

Figure 14. - Clean room.

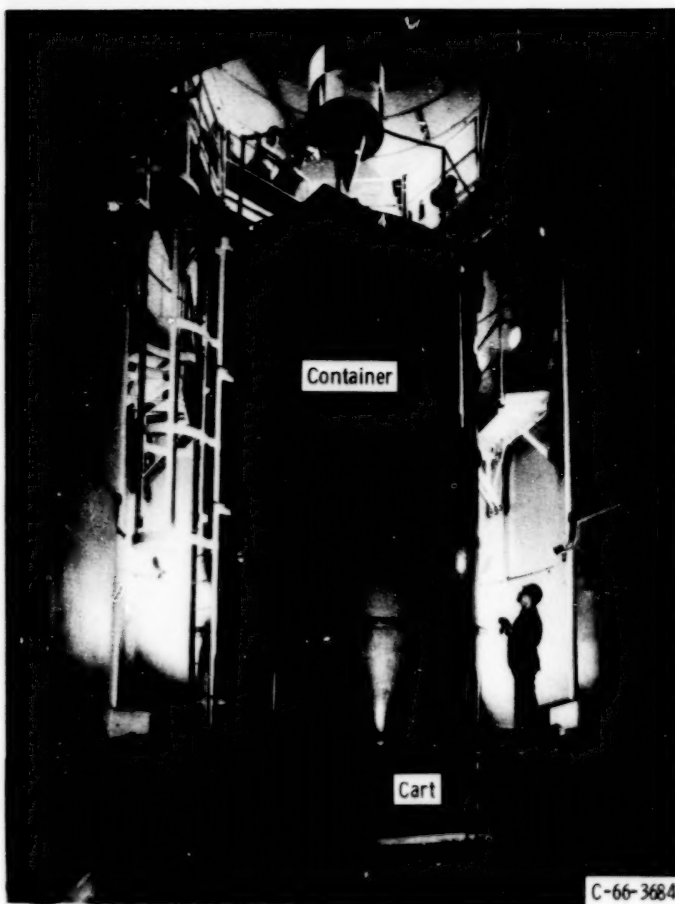


Figure 15. - Deceleration system.

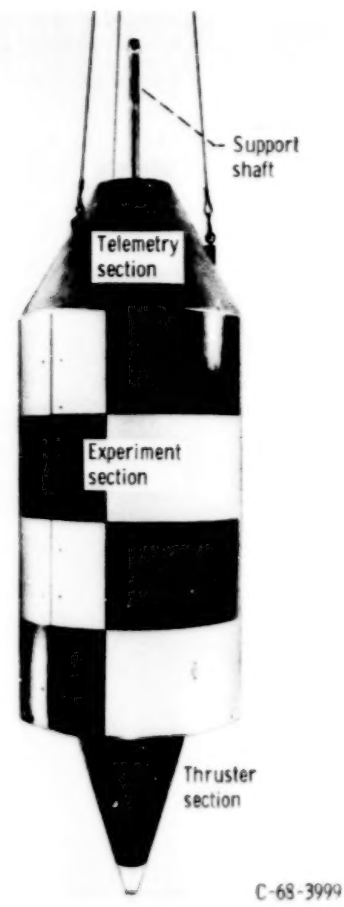


Figure 16. - Experiment vehicle.

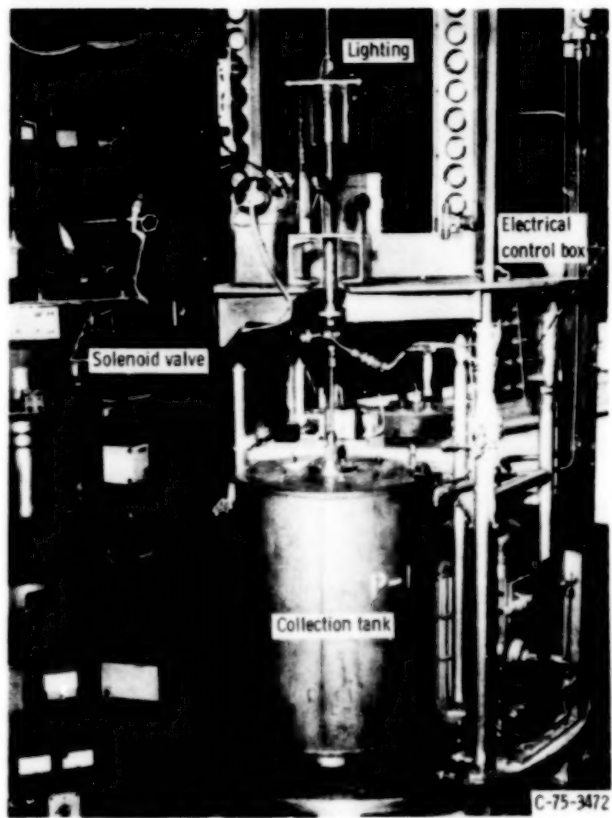


Figure 17. - Experiment package.

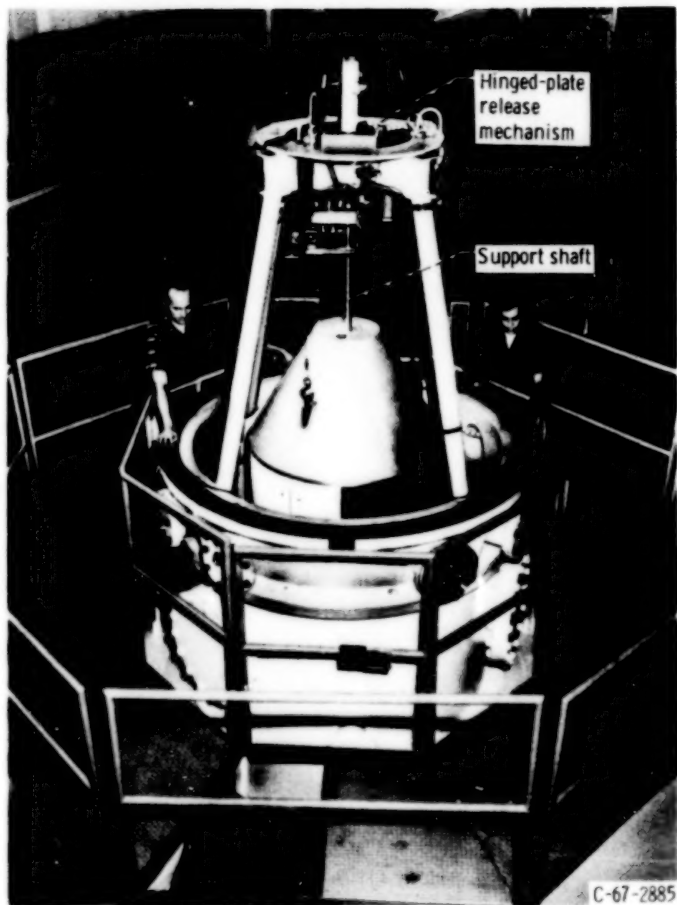


Figure 18. - Vehicle position prior to release.

1. Report No. NASA TP-1492	2. Government Accession No.	3. Recipient's Catalog No.	
4. Title and Subtitle CONTOURED TANK OUTLETS FOR DRAINING OF CYLINDRICAL TANKS IN LOW-GRAVITY ENVIRONMENT		5. Report Date July 1979	
7. Author(s) Eugene P. Symons		6. Performing Organization Code	
9. Performing Organization Name and Address National Aeronautics and Space Administration Lewis Research Center Cleveland, Ohio 44135		8. Performing Organization Report No. E-9969	
12. Sponsoring Agency Name and Address National Aeronautics and Space Administration Washington, D.C. 20546		10. Work Unit No. 506-21	
15. Supplementary Notes		11. Contract or Grant No.	
		13. Type of Report and Period Covered Technical Paper	
		14. Sponsoring Agency Code	
16. Abstract <p>An analysis is presented for defining the outlet contour of a hemispherical-bottomed cylindrical tank that will prevent vapor ingestion when the tank is drained. The analysis was used to design two small-scale tanks that were fabricated and then tested in a low-gravity environment in the Lewis Research Center's Zero Gravity Facility. The draining performance of the tanks was compared with that for a tank with a conventional outlet having a constant circular cross-sectional area, under identical conditions. Even when drained at off-design conditions, the contoured tank had less liquid residuals at vapor ingestion than the conventional-outlet tank. Effects of outflow rate, gravitational environment, and fluid properties on the outlet contour are discussed. Two potential applications of outlet contouring are also presented and discussed.</p>			
17. Key Words (Suggested by Author(s)) Fluid mechanics Weightlessness Draining		18. Distribution Statement Unclassified - unlimited STAR Category 34	
19. Security Classif. (of this report) Unclassified	20. Security Classif. (of this page) Unclassified	21. No. of Pages 45	22. Price* A03

